ELSEVIER

International Journal of Heat and Fluid Flow 21 (2000) 512–519

International Journal of HEAT AND FLUID FLOW

www.elsevier.com/locate/ijhff

Experimental study of a separating, reattaching, and redeveloping flow over a smoothly contoured ramp

Simon Song, David B. DeGraaff, John K. Eaton *

Department of Mechanical Engineering, Stanford University, Building 500, Stanford, CA 94305-3030, USA

Abstract

A turbulent boundary layer that separates, reattaches, and redevelops over a smoothly contoured ramp and a downstream flat plate has been examined. In order to resolve the flow in the viscous sublayer, a custom-built, two-dimensional LDA with a very high resolution was used. A small separation bubble occurred over the trailing edge of the ramp. The $\overline{v'v'}$ and $-\overline{u'v'}$ Reynolds stress components increased rapidly in the adverse pressure gradient boundary layer, and developed large outer layer peaks aligned with the inflection point in the mean velocity profile. The high stress levels were nearly unchanged by the reattachment process, decaying only after the mean velocity profile recovered and outer-layer production dropped. A key feature is that the inner layer recovered relatively quickly to a typical turbulent boundary layer in the redeveloping region, while the outer layer recovery was retarded by the large eddies generated in the separation region.

1. Introduction

The study of boundary layer separation, reattachment, and downstream recovery is important because the details of separated flows are difficult to predict, and they influence the performance of many common devices such as airfoils and diffusers. Separated flows have been the subject of experimental and computational research for decades because of their practical importance. The vast majority of the experimental studies involve separation from a sharp edge including backward-facing steps (cf. Eaton and Johnston, 1981; Troutt et al., 1984), flow over a blunt plate or cylinder (cf. Cherry et al., 1984; Sigurdson, 1995), and flow over a fence in front of a flat plate (cf. Ruderich and Fernholz, 1986; Hancock, 1999). While these flows offer important insight into the flow mechanisms in the separated flow, reattachment region, and downstream recovery, they give no information about the approach of the boundary layer to separation or possible couplings between the process of flow separation and the downstream recovery. By contrast, Simpson and co-workers (Simpson et al., 1981a,b; Shiloh et al., 1981) have examined the physics of boundary layers separating from a smooth wall without downstream reattachment or recovery. These studies do not address the possible effects of unsteadiness near reattachment having an upstream effect on the separating boundary layer.

There has been relatively little detailed study of a full separation bubble with downstream recovery to capture the interactions between the various regions of the flow. The blunt plate and fence flows have extremely thin boundary layers at separation so there is probably little influence of the upstream flow on the downstream development. On the other hand, Eaton and Johnston (1981) showed substantial effects of the upstream boundary layer on the downstream development in backward facing step flows. Castro and Epik (1998) concluded that the boundary layer recovery downstream of reattachment is essentially independent of the upstream conditions, i.e., a separation bubble is an overwhelming perturbation to the boundary layer (Bradshaw and Wong, 1972). The studies by Simpson's group showed that the large velocity fluctuations in the intermittent transitory detachment region and in the separation bubble were caused by separated shear layer eddies sweeping all the way down to the wall. This indicates that there is direct relationship between the turbulent eddies in the adverse pressure gradient boundary layer and in the separated shear layer.

Our goal is to provide detailed mean velocity and turbulence measurements in the vicinity of a separation bubble where separation and reattachment take place on smooth walls. We place particular emphasis on the recovering boundary layer because of several interesting and challenging features of this flow. At reattachment, the mean velocity profile has no logarithmic region and all of the turbulence stresses have large peaks away from the wall at a distance roughly corresponding to the height of the inflection point in the mean velocity profile. The mean profile recovers very rapidly downstream except for perturbations in the outer layer which persist for many boundary layer thicknesses downstream (Bradshaw and Wong, 1972). The turbulence profiles recover more slowly, apparently because of the persistence of separated shear layer eddies in the reattached boundary layer.

Many authors have pointed out that a boundary layer recovers from a perturbation by developing an internal layer which has standard boundary layer behavior and grows out

* Corresponding author.
E-mail address: eaton@vonkarman.stanford.edu (J.K. Eaton).

0142-727X/00/$ - see front matter
PII: S0142-727X(00)00039-4

through the perturbed layer (cf. Bradshaw and Wong, 1972; Bandyopadhyay and Ahmed, 1993; Webster et al., 1996). Alving and Fernholz (1996) and Castro and Epik (1998), however, suggested that the internal layer does not always appear in the recovery region. DeGraaff and Eaton (1999a) introduced the concept of a "stress equilibrium layer" which is a wall-adjacent region where the Reynolds stresses are in equilibrium with the local wall skin friction. They suggested that the extent of this region was dependent on the streamwise gradient of the skin friction and upstream history.

Computation of the recovering boundary layer appears to offer a strong challenge to existing CFD models because of the lack of equilibrium between the mean velocity profile and turbulent stresses. Large eddy simulation has been used to predict such flows at low Reynolds number (Ghosal et al., 1995). However, at high Reynolds number, near-wall models are necessary to avoid excessive grid requirements. It is important to determine if simple models developed for flat plate flows can represent the stress equilibrium layer in a recovering boundary layer. It thus appears critical to supply detailed data in the very near wall region of the recovering boundary layer.

A second objective of the work is to provide a well-qualified data set for testing both Reynolds-averaged and higher-order simulations. Simplicity of the boundary conditions is very important and the inlet geometry should be simple enough that time-dependent inlet conditions can be generated simply. In particular, we avoided opposite wall suction used to induce separation on flat plates in previous studies and used a flat plate boundary layer inlet flow. We have worked closely with modelers (Wasistho et al., 1999) to insure that the boundary conditions, and especially the inlet flow are sufficiently well defined. The flow geometry, selected after several CFD studies, has a flat plate turbulent boundary layer flowing down a smoothly contoured ramp onto a downstream flat plate. Separation occurs roughly halfway down the ramp, producing a relatively small separation bubble. The long flat plate downstream provides recovery towards a normal flat plate boundary layer.

2. Experimental set-up

The experiments were performed in the moderate-scale, closed-loop wind tunnel described by DeGraaff and Eaton (1999a). The tunnel has a test section 152 mm by 711 mm by 3.0 m long. Two honeycombs, three screens, and a 5:1 contraction are used to reduce the freestream turbulence intensity to approximately 0.2%. The boundary layer is tripped 150 mm downstream of the contraction exit. The two dimensionality of the flow was examined by measuring the streamwise mean and fluctuating velocity using a single-wire hot wire at several spanwise locations in the recovery region. The hot wire probe and procedure were the same as described in Webster et al. (1996). These measurements showed that the flow in the central region of the flow was spanwise uniform and was not affected by the side wall boundary layers. No significant 3D effects were expected since the ratio of spanwise width to separation bubble length is over 17. It is important to note that the flow is only two dimensional in the mean, and the turbulence is fully three-dimensional.

A special insert was placed into the rectangular test section to form the ramp geometry. The upstream end of the insert is a 169 mm long contraction reducing the test section height from 152 mm to 131 mm. There is then a 320 mm long flat section to allow the boundary layer to recover its equilibrium characteristics. The downstream end of the insert forms the test geometry as illustrated in Fig. 1. This geometry was designed to produce a small separation bubble using NASA's INS2D CFD

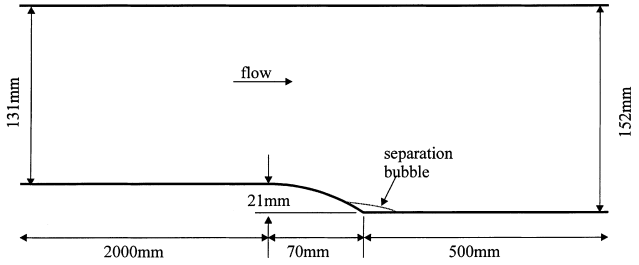

Fig. 1. Flow geometry. Ramp radius of curvature = 127 mm.

code supplemented with the v^2–f turbulence model developed by Durbin (1993). The boundary layer upstream of the ramp has a thickness of approximately 25.3 mm or approximately 1.2 times the height of the ramp. Therefore, while the separation bubble provides a large perturbation to the boundary layer, it is perhaps not an overwhelming perturbation in the sense of Bradshaw and Wong (1972).

A very high resolution measurement system is required in order to resolve the near-wall features of the separating and recovering boundary layers. We used the custom, two-component LDA system described by DeGraaff and Eaton (1999a). The system uses special transmitting optics and side scatter collection optics to achieve a measurement volume 35 μm in diameter and 60 μm in length. A comparison of the measurement volume size to a conventional miniature cross wire probe is shown in Fig. 2. The system uses frequency shift to separate the two velocity components and a single Macrodyne 3102 frequency domain processor to measure both velocity components simultaneously. This and the small measurement volume ensure that all two component velocity measurements are from the same tracer particle. The seeding system used 0.45 μm diameter polystyrene spheres injected into the tunnel with a water carrier via an airbrush in the tunnel return leg. Due to the small measurement volume, data rates are very low ranging from 15 to 25 samples/s. The height of the closest measurements to the wall is 80 μm corresponding to $y^+ = 3.5$.

The LDA data were corrected for velocity bias and validation bias using an experimental correction developed by DeGraaff and Eaton (1999b). This correction is based on direct measurement of the correlation between flow velocity and LDA sample rate. The corrected data have estimated

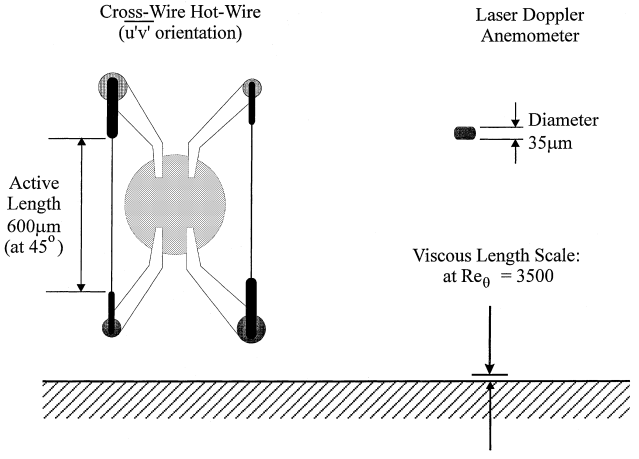

Fig. 2. Comparison of LDA and cross-wire hot wire measurement volumes.

uncertainties of ±1.5%, ±4%, ±8%, and ±10% for streamwise mean velocity (U), $\overline{u'u'}$, $\overline{v'v'}$, and, $\overline{u'v'}$, respectively.

Wall static pressure was measured through 0.635 mm diameter surface pressure taps using a Setra pressure transducer (Model 264) with the range of 0–25.0 in. of H_2O for both top and bottom walls. The estimated uncertainty was less than 0.5%.

3. Results

3.1. Mean flow

Data are presented in a coordinate system with x in the freestream direction, and y in the wall-normal direction. The y-axis is maintained vertical, and does not follow the curvature of the ramp. A normalized streamwise coordinate, $x' = (x - x_0)/l$, is also used, where x_0 corresponds to the beginning of the ramp and l is the ramp length. Measurements were acquired at 14 streamwise locations from $x' = -2.00$ to $x' = 7.00$ for $Re_{\theta,\mathrm{ref}} = 3500$. $Re_{\theta,\mathrm{ref}} = 3500$ is the momentum thickness Reynolds number evaluated at the reference station of $x' = -2.00$. This corresponds to a freestream velocity at the reference station of 20.4 m/s.

Fig. 3 shows the static pressure coefficient, $C_p = (P - P_{x'=-1.81})/(0.5\rho U_{\mathrm{ref}}^2)$, for both the tunnel top and bottom walls, where ρ is the air density and U_{ref} is the free-stream velocity at the reference station. On the bottom wall, there is a strong favorable pressure gradient approaching the ramp up to $x' = 0.16$ due to the wall curvature effect. After that point, the flow expansion dominates, causing a strong adverse pressure gradient over the rest of the ramp. There is a short plateau around the trailing edge of the ramp, $x' = 1.00$. This indicates the presence of a separation bubble over the trailing edge as sketched in Fig. 1. The dividing streamline of the separation bubble acts like a flat wall over a short length around the trailing edge. The adverse pressure gradient region extends to $x' = 2.00$. The boundary layer displacement thickness drops rapidly after the trailing edge of the ramp, resulting in the mild favorable pressure gradient at $x' = 2.00$, after which it relaxes back to nearly zero pressure gradient. The results of the static pressure on the top wall reveal that there is no separation on the top wall and show the static pressure increases monotonically over the ramp.

Fig. 4 shows the mean streamwise velocity development. The figure is drawn to scale, with the vertical axis expanded by a factor of two relative to the horizontal axis in order to see the near wall region more clearly. Integral parameters for the profiles shown are compiled in Table 1. The acceleration

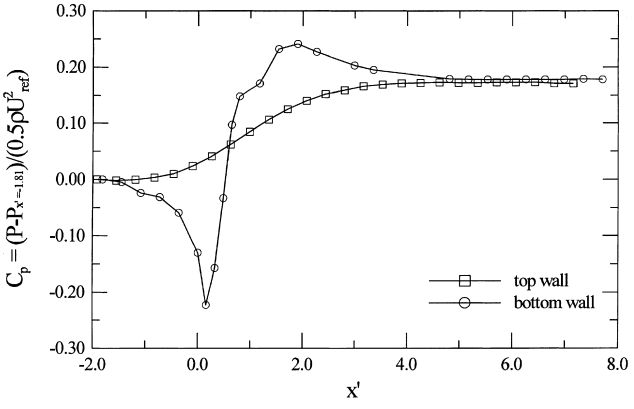

Fig. 3. Wall static pressure measurements.

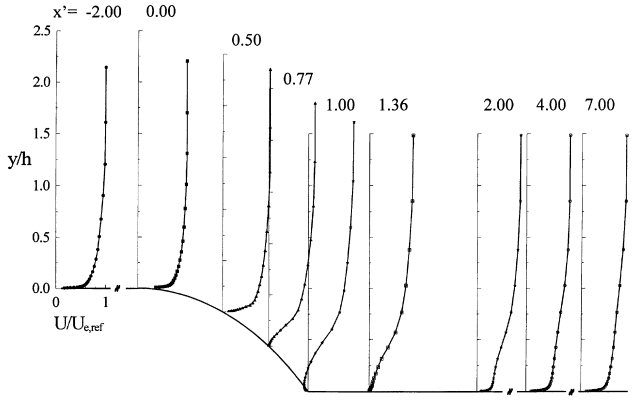

Fig. 4. Streamwise mean velocity development.

parameter, $\Delta_p = -v(\mathrm{d}p/\mathrm{d}x)/\rho u_\tau^3$, evaluated using the maximum adverse pressure gradient and the reference integral parameters is −0.06. The curvature parameter $\delta_{99,x'=0.00}/R$ is 0.18. This means that the boundary layer is subject both to strong adverse pressure gradient and strong convex curvature.

The curvature of the ramp produces a favorable pressure gradient up to $x' = 0.16$, which causes the boundary layer to thin. Once in the adverse pressure gradient, the boundary layer thickness grows rapidly and the profiles develop an inflection point. The boundary layer separates at $x' = 0.77$ and reattaches at $x' = 1.36$. The horizontal length of the separation bubble is 41 mm. The height of the separation bubble, which is defined to be where the mean velocity is equal to zero, is 4.7 mm at the trailing edge. The back flow in the separation bubble is clearly visible at the trailing edge.

The mean flow recovery is very rapid downstream of reattachment. By $x' = 2.00$, the profile has filled out considerably, although it still shows a significant deficit in the outer layer. The mean profiles at $x' = 4.00$ and 7.00, however, have essentially recovered nearly to a flat plate boundary layer. This can clearly be recognized in the log law plot of Fig. 5. The standard log law (solid line) was plotted using $\kappa = 0.41$ and $B = 5.0$. For each profile, the friction velocity was calculated from the log law, but it would not be much different from what we get from independent measurements of skin friction. The wall shear stresses directly calculated from sublayer velocity measurements was within 2.8% and 6.7% of the values from the log law for $x' = 4.00$ and 7.00, respectively. The profile of $x' = 4.00$ has a dip below the standard log law value, which is a typical behavior of recovering boundary layer as first noted by Bradshaw and Wong (1972). At $x' = 7.00$, the log law profile is almost fully recovered.

3.2. Reynolds stresses

The streamwise normal stress is plotted on a linear scale in Fig. 6 to illustrate the overall development of the turbulence field. Note that this stress component is normalized as $\overline{u'u'}/(U_e U_\tau)_{\mathrm{ref}}$ and the reference station is $x' = -2.00$. DeGraaff and Eaton (1999a) showed that this scaling collapses flat plate boundary layer data over a wide range of Reynolds numbers. A fixed scaling based on the reference values is used for two reasons. First, the fixed scaling shows absolute variations of the stress level through the flow field, in particular, the rapid growth on the upstream half of the ramp. Also, the local value of U_τ is not an appropriate scale in the separated flow region where the skin friction passes through zero.

Fig. 6 shows that the streamwise normal stress develops a large peak near the inflection point in the mean velocity

Table 1
Integral parameters; δ_{99} 99% boundary layer thickness, δ^* displacement thickness, θ momentum boundary layer thickness, H shape factor, G Clauser shape factor, $Re_{\delta 99}$, $Re_{\delta *}$, Re_{θ}, Reynolds numbers based on local freestream velocity for respective length scale

x'	x (mm)	δ_{99} (mm)	δ^* (mm)	θ (mm)	H	G	$Re_{\delta 99}$	$Re_{\delta *}$	Re_{θ}
−2.00	−140	25.3	3.4	2.6	1.32	5.85	33880	4600	3500
0.00	0	22.2	2.4	1.9	1.28	4.75	29720	3200	2500
0.50	35	25.0	3.7	2.6	1.44		32370	4800	3300
0.57	40	26.8	4.4	3.0	1.50		34730	5800	3800
0.64	45	29.1	5.6	3.4	1.67		37050	7100	4300
0.77	54	34.0	8.3	3.9	2.13		42890	10500	4900
0.89	62	39.0	11.6	4.2	2.74		49520	14800	5400
1.00	70	45.8	15.7	4.5	3.47		57170	19500	5600
1.25	87.5	57.0	14.1	5.3	2.66		70120	17300	6500
1.36	95.2	57.7	13.2	5.6	2.34		70570	16100	6900
1.43	100	58.2	12.8	5.8	2.20		71920	15800	7200
2.00	140	42.0	9.7	5.5	1.74		50060	11500	6600
4.00	280	39.5	7.2	5.0	1.44	8.34	48120	8800	6100
7.00	490	37.3	6.8	4.9	1.39	7.49	44930	8200	5900

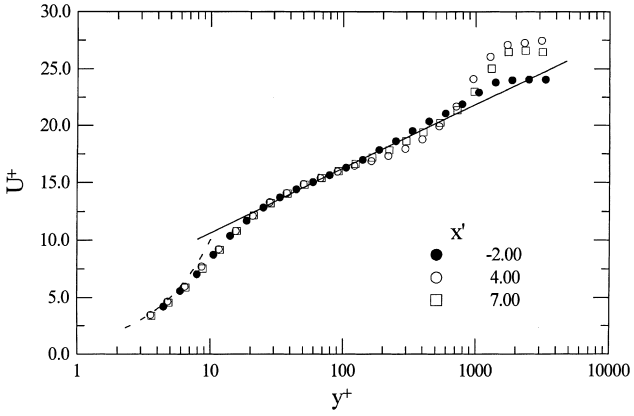

Fig. 5. Law of the wall for flat plate profiless.

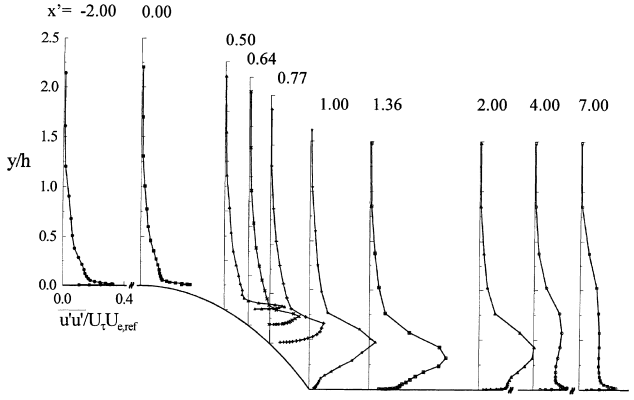

Fig. 6. Streamwise Reynolds normal stress development: $\overline{u'u'}$ is normalized by $U_\tau U_{e,ref}$ and $x' = -2.00$ is the reference station.

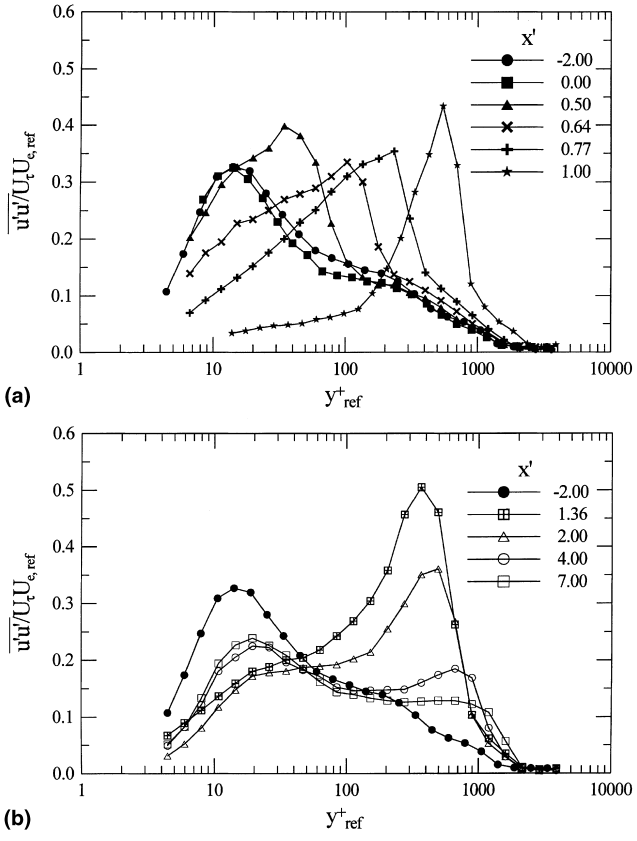

Fig. 7. Streamwise Reynolds normal stress normalized by $U_\tau U_{e,ref}$.

profiles. This peak is still very strong at $x' = 2.00$, well downstream of reattachment. The peak decays and diffuses outward as the flow proceeds downstream. The near wall peak is reestablished in the profile at $x' = 4.00$, but there is still a significant outer layer peak. By $x' = 7.00$, the turbulence is essentially recovered near the wall, and the outer layer peak has decayed to form a plateau of constant normal stress. These recovering boundary layer results will be discussed in more detail below.

Selected profiles of the Reynolds stresses are shown in Figs. 7–9: the streamwise normal stress, $\overline{u'u'}$ in Fig. 7, the wall normal stress, $\overline{v'v'}$ in Fig. 8, and the Reynolds shear stress, $-\overline{u'v'}$ in Fig. 9. The first figure in each pair shows the profiles on the ramp itself to show the development of the stresses through separation. The second figure shows the stresses on the recovery plate including the reattachment point and the downstream redevelopment. The upstream reference profile is shown on both plots for comparison. These stresses are plotted in semi-logarithmic coordinates using the reference velocity scales at $x' = -2.00$ to normalize them. This is done to

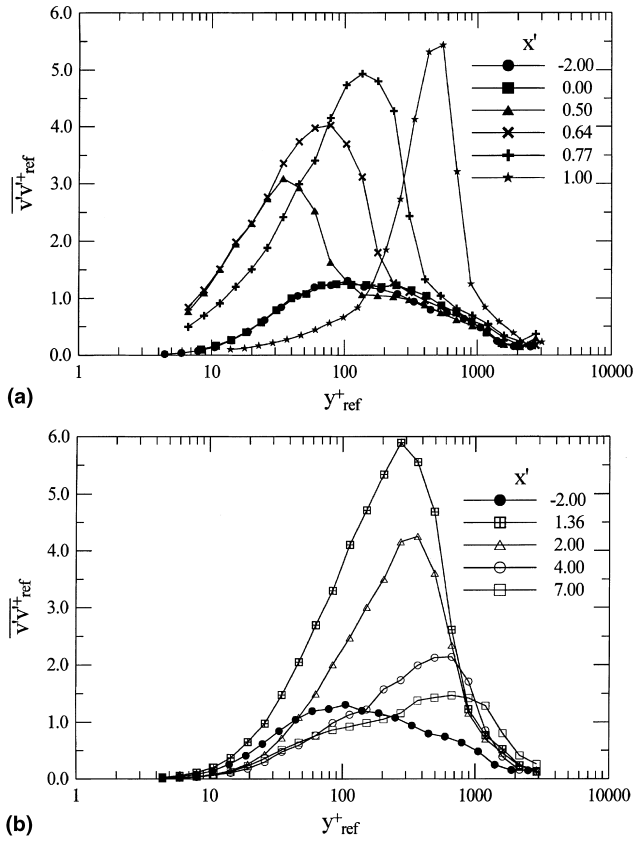

Fig. 8. Wall normal Reynolds stress normalized by $U^2_{\tau,ref}$.

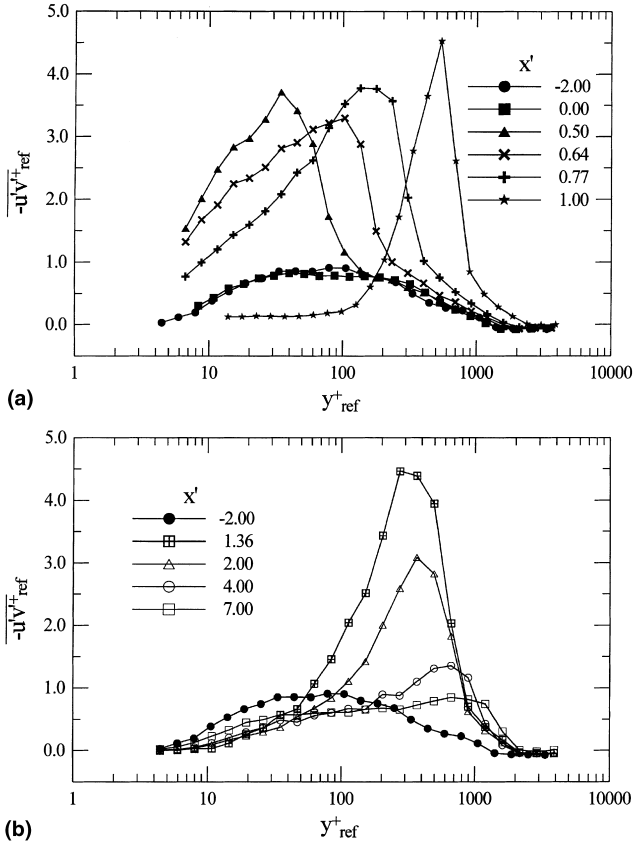

Fig. 9. Reynolds shear stress normalized by $U^2_{\tau,ref}$.

emphasize the near-wall region while maintaining fixed scaling. The scaling shown collapses profiles of these quantities over a wide range of Reynolds numbers in flat plate boundary layers (DeGraaff and Eaton, 1999a).

The boundary layer turbulence is strongly modified in the adverse pressure gradient region upstream of separation. The peak level of the streamwise normal stress increases quickly to a level about 25% higher than the upstream boundary layer. By contrast, the peak levels of the Reynolds shear stress and the wall normal stress increase by factors of 3–5 over the upstream levels. The peak levels of the wall normal stress continue to increase approaching separation as opposed to the streamwise normal stress and the shear stress which increase rapidly to an elevated level then remain nearly constant. For all three stress components, the peaks shift outward moving downstream remaining in alignment with the inflection point in the mean profile. This is demonstrated for the Reynolds shear stress in Fig. 10, where the y-coordinate is normalized by the height of the inflection point.

The effects of the mean profile distortion by the adverse pressure gradient appear to overwhelm the effects of convex curvature upstream of separation. One might expect that the strong curvature would cause rapid suppression of the turbulence in the outer layer (Wyngaard et al., 1968; Gillis and Johnston, 1983). However, the present measurements show that the outer layer turbulent stresses either remain nearly constant or increase slowly approaching separation. Even by the separation point, the effects of the ramp are confined to what was the logarithmic region of the boundary layer. The wake region is virtually unaffected by the presence of the ramp. This changes after separation. By the middle of the separation bubble, there is a large peak in what was the wake region of the boundary layer, and the Reynolds stresses are increased all the way to the outer edge of the boundary layer.

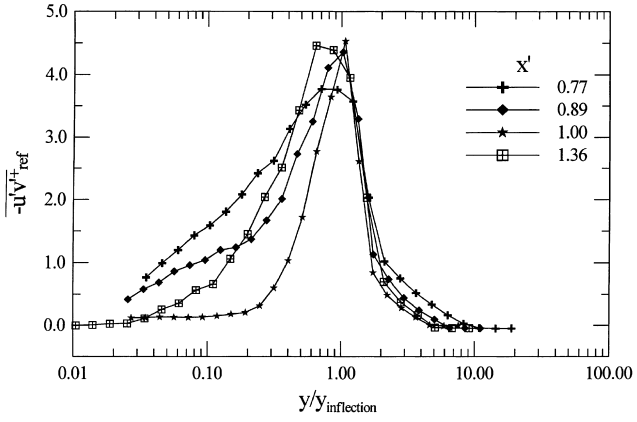

Fig. 10. Reynolds shear stress: y-coordinate scaled on the height of the inflection point in the mean profile.

The profiles at $x' = 1.00$ are in the center of the separation bubble and have a different character than the distorted boundary layer profiles upstream. All three measured stress components are relatively small within the separation bubble, but the shear stress is smaller than the normal stress components. While the turbulence is energetic, it is uncorrelated showing that the turbulence stresses are caused by inactive motions imposed by the active separated shear layer passing above (Simpson et al., 1981a; Adams and Johnston, 1988).

The Reynolds stress levels reach maximum values near reattachment at $x' = 1.36$. Comparing the profiles at reattachment to those in the fully separated flow ($x' = 1.00$), we see that the peaks in all stresses at reattachment are either equal to or higher than at $x' = 1.00$. This is in contrast to the backward-facing step flows surveyed by Eaton and Johnston (1981) which usually show that the Reynolds stresses begin to decay approximately one step height upstream of reattachment.

Downstream recovery of the Reynolds stresses is shown in Figs. 7(b), 8(b) and 9(b). The most obvious feature of the recovery is that the outer layer peak of all Reynolds stress components decays rapidly and moves slowly outward. The formation of a stress equilibrium layer is first evident at $x' = 2.00$, where a near wall peak in the streamwise normal stress is first evident. A stress equilibrium layer is defined in DeGraaff and Eaton (1999a) to mean a region where all the flow quantities collapse onto the profiles of a zero-pressure-gradient flat-plate boundary layer, when normalized by local scaling. Moving farther downstream to $x' = 4.00$, all the stress components begin to take on more standard profile shapes, although there are still very significant outer layer peaks, especially of $\overline{v'v'}$. By the final measurement station a stress equilibrium layer has been reestablished extending out to about $y^+_{ref} = 100$. This is shown more clearly in Figs. 11(a) and (b) which compare the most upstream and downstream profiles ($x' = -2.00$ and $x' = 7.00$) when local values of the scaling variables are used. An excellent collapse is seen out to $y^+ = 100$. Beyond that point, the plateau in $\overline{u'u'}$ and the peak in $\overline{v'v'}$ and $-\overline{u'v'}$ show that the outer layer is still far out of equilibrium with the wall shear stress. Alving and Fernholz (1996) showed that skin friction recovers to normal values for a canonical boundary layer at the same Reynolds number within five separation bubble lengths downstream of reattachment. This corresponds to $x' = 4.3$ in the present case. The present data indicate that both the near wall mean and turbulence profiles have returned to normal by this point.

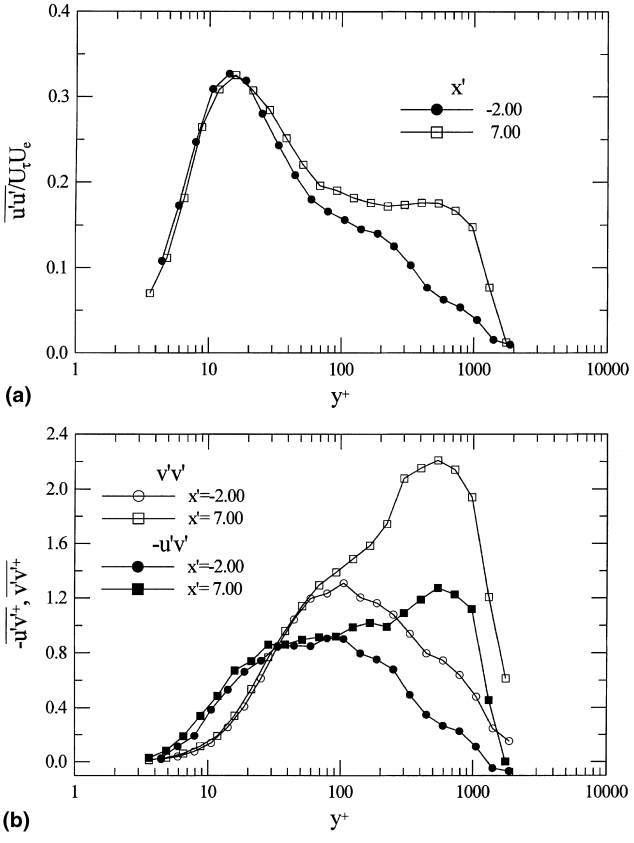

Fig. 11. Comparison of Reynolds stresses for $x' = -2.00$ and 7.00.

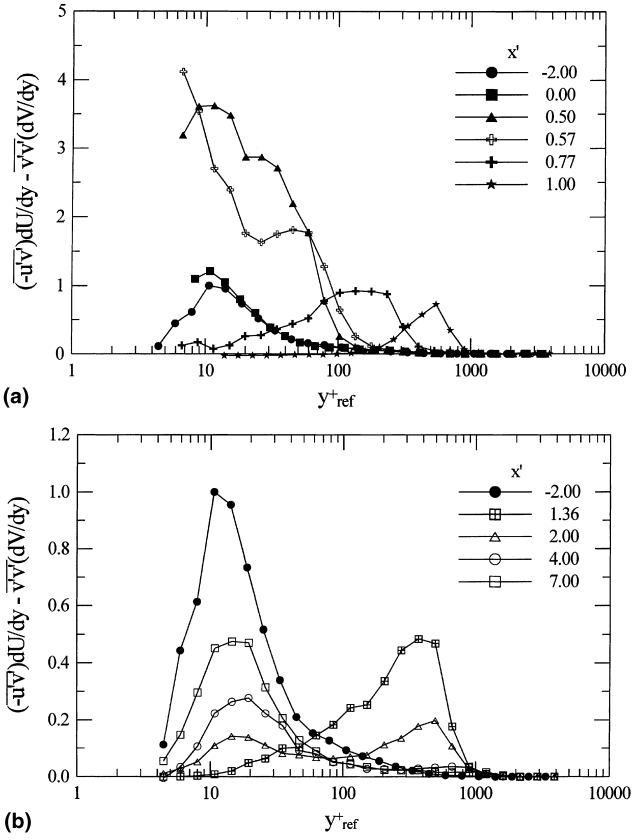

Fig. 12. Production of turbulent kinetic energy normalized by maximum production value at $x' = -2.00$.

Figs. 12 (a) and (b) show the production of turbulent kinetic energy normalized by the maximum production value at $x' = -2.00$. At the onset of the adverse pressure gradient, there is a very large peak in the production near the wall corresponding to the rapid growth of the Reynolds stresses. At separation, the production peak moves outward into the separated shear layer with virtually zero production near the wall. This corroborates the earlier conclusion that the turbulence within the separation bubbles is inactive. The peak level of the production in the separated shear layer is much smaller than in the adverse pressure gradient boundary layer, but the production is spread over a much wider region of the flow. A weak production peak persists in the outer layer through $x' = 2.00$. However, there is no significant production in the outer layer at $x' = 4.00$ and 7.00. This shows clearly the non-equilibrium nature of the recovering boundary layer. The outer layer peak in the recovering layer is simply the decaying remnants of the separated shear layer turbulence. The slow decay of the Reynolds stresses in this remnant, in spite of the complete absence of any production, indicates that the turbulence has a very long time scale as would be characteristic of free-shear-layer turbulence.

4. Discussion

Te present data which include highly resolved near-wall measurements in the recovery region allow us to answer an open question regarding recovering boundary layers. Alving and

Fernholz (1996) and Castro and Epik (1998) argued that the internal layer in the recovering boundary layer downstream of reattachment does not have the same characteristics as the near-wall region of a canonical boundary layer. Castro and Epik hypothesized that "the inner layer could not possibly develop normally until the outer flow has become more normal". However, in earlier work Bradshaw and Wong (1972) and Jovic (1993) concluded that the inner layer re-developed the canonical form more rapidly than the perturbed outer layer. DeGraaff and Eaton (1999a) studying a boundary layer recovering from a region of strong adverse pressure gradient without separation found that the inner layer began recovering its canonical form as soon as $d\tau/dx$ recovered towards flat plate values.

In the present experiments, we have shown that the inner layer below $y^+ = 100$ recovers normal boundary layer characteristics by $x' = 7.00$, while the outer layer is still distorted by energetic large eddies. The first evidence of the growing stress equilibrium layer appears very near the wall at $x' = 2.00$. By $x' = 7.00$ the inner layer below $y^+ = 100$ has a mean profile which follows the log law and Reynolds stresses which are in equilibrium with the local wall shear stress. Other structural parameters not shown here including the anisotropy parameter $(\overline{v'v'}/\overline{u'u'})$ and $(-\overline{u'v'})/(\overline{u'u'} + \overline{v'v'})$ also have recovered to canonical form in the inner layer. A critical factor appears to be the drop in turbulence production in the outer layer to levels well below the near-wall peak. While there are still large, energetic eddies in the outer layer, they appear to be inactive, having no effect on the turbulence in the stress equilibrium layer. This conclusion may not hold for cases in which the separation bubble height is much greater than the upstream boundary layer thickness. High resolution measurements and correct normalization of the stresses are needed to determine if this conclusion can be extended to such cases of overwhelming perturbation.

Our conclusions about the stress equilibrium layer offer experimental support for techniques such as high Reynolds number large eddy simulation and detached eddy simulation which use canonical models for the near wall region. When the Reynolds stresses are scaled correctly, they are seen to recover quite quickly to the canonical profiles. What is unknown at this point is what controls the growth rate of the stress equilibrium layer. Better spatial resolution in the streamwise direction and accurate measurements of the wall shear stress are needed to resolve that question for the present flow.

Another open question in turbulent reattaching flows is the fate of the separated shear layer eddies as they pass through the reattachment zone. Previous conclusions range from the eddies being torn roughly in two near reattachment to the eddies passing roughly unmodified over the top of the reattachment zone. To add some additional insight into this question, we have acquired detailed stress measurements at three closely spaced stations centered on the reattachment point. The streamwise extent from $x' = 1.25$ to $x' = 1.43$ comprises approximately 1/3 of the length of the separation bubble. Fig. 13 shows the streamwise normal stress for these three profiles demonstrating that it is virtually unchanged through the reattachment zone. Since the profiles are dominated by the large outer layer peak associated with the separated shear layer eddies, we can conclude that these eddies are essentially unmodified by their interaction with the wall. This conclusion is probably not universal. Measurements in other reattaching flows have shown that the Reynolds stresses begin to decay at the upstream edge of the reattachment zone.

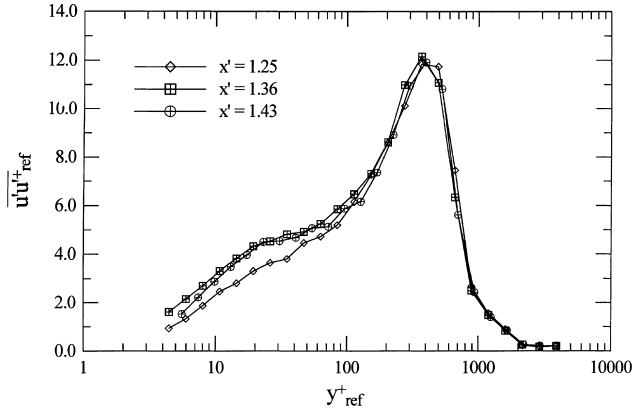

Fig. 13. Comparison of Streamwise normal stress profiles in reattachment zone.

5. Summary and conclusions

Experimental measurements are presented for a boundary layer separating from a smoothly contoured plate with reattachment and subsequent recovery on a downstream flat plate. The wall normal stress and the shear stress grow rapidly in the adverse pressure gradient region upstream of separation forming a large peak above the wall. The streamwise normal stress grows more slowly, but still forms a significant peak coincident with the other peaks and with the inflection point in the mean velocity profile. The Reynolds stress profiles remain approximately constant across the separated flow region with a region of inactive turbulence near the wall and an active separated shear layer above. The Reynolds stress peaks are not significantly altered by reattachment, until the turbulence production rate drops as the mean profile recovers its normal boundary layer form.

The recovering boundary layer behaves in a similar fashion to the more mildly perturbed layer studied by DeGraaff and Eaton (1999a). This indicates that the development of a stress equilibrium layer is a universal feature of recovering boundary layers, and that universal near wall models may provide an accurate representation of recovering flows. What is not known yet is what determines the rate at which the stress equilibrium layer grows and brings the outer layer back into equilibrium. In the present case, energetic but inactive eddies persist in the outer layer to the end of the test section. The associated Reynolds stress peaks decay after the mean velocity profile recovers reducing the turbulence production in the outer layer to normal levels. However, the decay rate appears to be considerably slower than in the non-separated experiments of DeGraaff and Eaton (1999a).

Acknowledgements

We gratefully acknowledge financial support from The Office of Naval Research, under grant N00014-94-1-0070 supervised by Dr. Pat Purtell and Dr. Candace Wark. Simon Song was partially supported by a Stanford Graduate Fellowship.

References

Adams, E.W., Johnston, J.P., 1988. Flow structure in the near wall zone of a turbulent separated flow. AIAA J. 26 (8), 932.

Alving, A.E., Fernholz, H.H., 1996. Turbulent measurements around a mild separation bubble and downstream of reattachment. J. Fluid Mech. 322, 297.

Bandyopadhyay, P.R., Ahmed, A., 1993. Turbulent boundary layers subjected to multiple curvatures and pressure gradients. J. Fluid Mech. 246, 503.

Bradshaw, P., Wong, F.Y.F., 1972. The reattachment and relaxation of a turbulent shear layer. J. Fluid Mech. 52, 113.

Castro, I.P., Epik, E., 1998. Boundary layer development after a separated region. J. Fluid Mech. 374, 91.

Cherry, N.J, Hillier, R., Latour, M.E.M., 1984. Unsteady measurements in a separated and reattaching flow. J. Fluid Mech. 144, 13.

DeGraaff, D.B., Eaton, J.K., 1999a. Reynolds number scaling of the turbulent boundary layer on a flat plate and on swept and unswept bumps, Rept. TSD-118, Stanford University, Stanford, CA, USA.

DeGraaff, D.B., Eaton, J.K., 1999b. A high-resolution Laser Doppler Anemometer: design, qualification, and uncertainty. Exp. Fluid (submitted).

Durbin, P., 1993. Application of a near-wall turbulence model to boundary layers and heat transfer. Inter. J. Heat and Fluid Flow 14 (4), 316.

Eaton, J.K., Johnston, J.P., 1981. A review of research on subsonic turbulent flow reattachment. AIAA J. 19 (9), 1093.

Ghosal, S., Lund, T.S., Moin, P., Akselvoll, K., 1995. Dynamic localization model for large-eddy simulation of turbulent flows. J. Fluid Mech. 286, 229.

Gillis, J.C., Johnston, J.P., 1983. Turbulent boundary-layer flow and structure on a convex wall and its redevelopment on a flat wall. J. Fluid Mech. 135, 123.

Hancock, P.E., 1999. Measurement of mean and fluctuating wall shear stress beneath spanwise-invariant separation bubbles. Exp. Fluids 27, 53.

Jovic, S., 1993. An experimental study on the recovery of a turbulent boundary layer downstream of reattachment. In: Rodi, W., Martelli, F. (Eds.), Engineering Turbulence Modeling and Experiment, Elsevier, Amsterdam, vol. 2, p. 509.

Ruderich, R., Fernholz, H.H., 1986. An experimental investigation of a turbulent shear flow with separation, reverse flow, and reattachment. J. Fluid Mech. 163, 283.

Shiloh, B.H., Shivaprasad, B.G., Simpson, R.L., 1981. The structure of a separating turbulent boundary layer. Part 3. Transvers velocity measurements. J. Fluid Mech. 113, 75.

Sigurdson, L.W., 1995. The structure and control of turbulent reattaching flow. J. Fluid Mech. 298, 139.

Simpson, R.L., Chew, Y.T., Shivaprasad, B.G., 1981a. The structure of a separating turbulent boundary layer. Part 1. Mean flow and Reynolds stresses. J. Fluid Mech. 113, 23.

Simpson, R.L., Chew, Y.T., Shivaprasad, B.G., 1981b. The structure of a separating turbulent boundary layer. Part 2. Higher-order turbulence results. J. Fluid Mech. 113, 53.

Troutt, T.R., Scheelke, B., Norman, T.R., 1984. Organized structures in a reattaching separated flow field. J. Fluid Mech. 143, 413.

Wasistho, B., Song, S., Squires, K.D., Eaton, J.K., 1999. Numerical study on recovery of ramp separation. Bull. Am. Phys. Soc. 44 (8) 106.

Webster, D.R., DeGraaff, D.B., Eaton, J.K., 1996. Turbulence characteristics of a boundary layer over a two-dimensional bump. J. Fluid Mech. 320, 53.

Wyngaard, J.C., Tennekes, H., Lumley, J.L., Margolis, D.P., 1968. Structure of turbulence in a curved mixing layer. Phys. Fluids 11, 1251.